Electronic and magnetic structures of the rare-earth permanent magnet $Nd_2Fe_{14}B$

B. I. Min
Department of Physics, Pohang Institute of Science and Technology, Pohang 790-600, Korea

J.-S. Kang, J. H. Hong, J. I. Jeong, Y. P. Lee, S. D. Choi, W. Y. Lee, and C. J. Yang
Research Institute of Industrial Science and Technology, Pohang 790-600, Korea

C. G. Olson
Ames Laboratory, Iowa State University, Ames, Iowa 50011
(Received 11 January 1993; revised manuscript received 1 June 1993)

Electronic and magnetic structures of $Nd_2Fe_{14}B$ are investigated by performing self-consistent local-density-approximation band-structure calculations and photoemission-spectroscopy (PES) measurements. Employing the linear muffin-tin-orbital band method, we have obtained electronic band structures for both paramagnetic and ferromagnetic phases of $Nd_2Fe_{14}B$, and compared the calculated density of states (DOS) with the experimental data obtained from PES measurements. It is found that B atoms contribute to the stabilization of the structure and substantially reduce the magnetic moment of neighboring Fe atoms through a hybridization interaction. The average magnetic moment of Fe atoms in the ferromagnetic phase is estimated to be $2.15\mu_B$. Depending on the distances from B atoms, Fe atoms at the j_2 site and those at the e site have the largest and smallest magnetic moments, respectively, in qualitative agreement with the experimental trend. The valence-band PES measurements for Nd $4f$ states indicate that the Nd valence is close to trivalent, with negligible Nd $4f$ spectral intensity close to E_F, which is consistent with the observed trivalent Nd $4f$ magnetic moments in this compound. The line shape of the Nd $4f$ PES is broader than that of pure Nd metal, reflecting effects of the hybridization between Nd $4f$ and Fe $3d$ electrons. The Fe $3d$ PES spectrum shows that the Fe $3d$ electrons mainly determine the DOS near E_F. The calculated Fe $3d$ projected local density of states agrees reasonably well with the Fe $3d$ PES spectrum, which implies that the Fe $3d$ magnetism in $Nd_2Fe_{14}B$ may well be understood in terms of the itinerant magnetism of Fe $3d$ electrons.

I. INTRODUCTION

A recently discovered rare-earth permanent magnet (REPM), $Nd_2Fe_{14}B$, has attracted great interest for its potential applications.[1–4] $Nd_2Fe_{14}B$ has larger energy products than $SmCo_5$, the existing typical REPM. Furthermore, Nd and Fe are more abundant in nature and so they are cheaper than Sm and Co. Considering its technological importance, it is necessary to understand the microscopic origin of the magnetism in $Nd_2Fe_{14}B$.

There have been several reports on the electronic structure of $Nd_2Fe_{14}B$. Inoue and Shimizu,[5] Itoh *et al.*,[6] and Szpunar, Wallace, and Szpunar[7] used a semiempirical tight binding and the recursion method and found that Fe atoms at the $j2$ site have the largest magnetic moments. Gu and Ching[8] and Zhong and Ching[9] have studied extensively the electronic structures of $Nd_2Fe_{14}B$ using the non-self-consistent orthogonalized linear combination of atomic orbitals (OLCAO) band method. They provided contour maps of the charge and spin densities of $Nd_2Fe_{14}B$ and also calculated the local orbital moments of Fe atoms. Sellmyer *et al.*[10] and Jaswal[11] have performed band calculations on $Y_2Fe_{14}B$ and $Nd_2Fe_{14}B$, using the self-consistent linearized muffin-tin-orbital (LMTO) band method.[12] Sellmyer *et al.* also compared the theoretical results with photoelectron spectroscopy (PES) measurements. More recently, Nordstroem, Johansson, and Brooks[13] also reported calculated magnetic moments of $Nd_2Fe_{14}B$ using the self-consistent LMTO band method.

In this paper, we present the results of self-consistent band-structure calculations and PES measurements of $Nd_2Fe_{14}B$. We have compared the calculated projected local density of states (PLDOS) with the measured PES spectra. Energy-band structures and density of states (DOS) have been obtained self-consistently for both paramagnetic and ferromagnetic phases by employing the LMTO band method and the Gaussian broadening method,[14] respectively. The von Barth–Hedin form for the electron-electron exchange correlation has been utilized in the local spin-density-functional approximation.[15] For the PES measurements on $Nd_2Fe_{14}B$, as compared to the previous work by Sellmyer *et al.*, the differences in this work are (i) our PES data are obtained from the surfaces free of O and/or C contamination, (ii) we have separated Nd $4f$ and Fe $3d$ emissions using the photon energy dependence of the photoionization cross sections, and (iii) we have fitted the extracted Nd $4f$ PES spectrum using the $4f^2$ final-state multiplet structures.

This paper is organized as follows. In Sec. II, the crystal structures of $Nd_2Fe_{14}B$ are briefly described and the

 ©1993 The American Physical Society

electronic structures from the spin-unpolarized and spin-polarized band calculations are discussed. In Sec. III, the experimentally determined Nd $4f$ PES spectra are presented and analyzed using the final-state multiplet structures. In Sec. IV, Fe $3d$ PES are compared with the theoretical PLDOS. Finally, a conclusion is summarized in Sec. V.

II. ELECTRONIC STRUCTURES

A. Computational details

Let us describe briefly the band method we have used and the crystal structure of $Nd_2Fe_{14}B$ for the later discussion of its electronic and magnetic structures. The LMTO band calculations carried out in this work are in principle similar to those of Jaswal[11] and Nordstroem, Johansson, and Brooks,[13] but our calculations are different in the following aspects. In the works of Jaswal and Nordstroem, Johansson, and Brooks, the Nd f electrons are treated as core electrons. Jaswal used a frozen-core approximation for f electrons, and so their electronic structures are not calculated self-consistently and the spin polarization of f electrons is not considered. Nordstroem, Johansson, and Brooks treated the $4f$ shell within a Russel-Saunders coupling and then fixed the occupation numbers for the majority and minority spins of f core electrons. In this work, the Nd f electrons are considered as valence electrons and are treated self-consistently, with the aim of studying the magnetic properties of Nd f electrons more clearly. In fact, we have also considered the case of treating Nd f electrons as core electrons for comparison and have obtained results similar to previous ones. Furthermore, we have used a larger LMTO basis set for Nd atoms and more k points for the Brillouin-zone integration to achieve more precise calculations.

$Nd_2Fe_{14}B$ has a tetragonal crystal structure, which belongs to the D_{4h}^{14} space group (see Fig. 2 of Ref. 4). The structure is very complicated, with four formula units of $Nd_2Fe_{14}B$, corresponding to 68 atoms, per unit cell. In one unit cell, there are two kinds of 8 Nd atoms, labeled as Nd(f) and Nd(g), respectively, six kinds of 56 Fe atoms, labeled as Fe(c), Fe(e), Fe(j_1), Fe(j_2), Fe(k_1), Fe(k_2), respectively, and only one kind of 4 B atoms, labeled as B(g). Near-neighbor Fe-Fe distances in the structure are between 2.4 and 2.8 Å. B atoms are known to play an important role in bonding,[4] since they occupy the centers of the trigonal prisms which are formed by 6 near neighbor Fe atoms [2 Fe(e) and 4 Fe(k_1) atoms] (see Fig. 1). Three Nd atoms are bonded to each B atom through the three vertical prism faces. Such a prism structure provides the basic frame for $Nd_2Fe_{14}B$, which connects all the Nd, Fe, and B atoms.

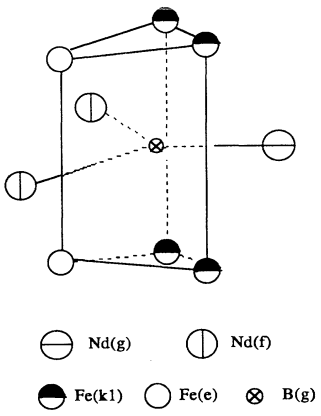

FIG. 1. Trigonal prism structure in the $Nd_2Fe_{14}B$, which includes Nd(f), Nd(g), Fe(k_1), Fe(e), and B.

B. Spin-unpolarized calculation

Figure 2 provides calculated total density of states (DOS) and the angular-momentum-projected local DOS

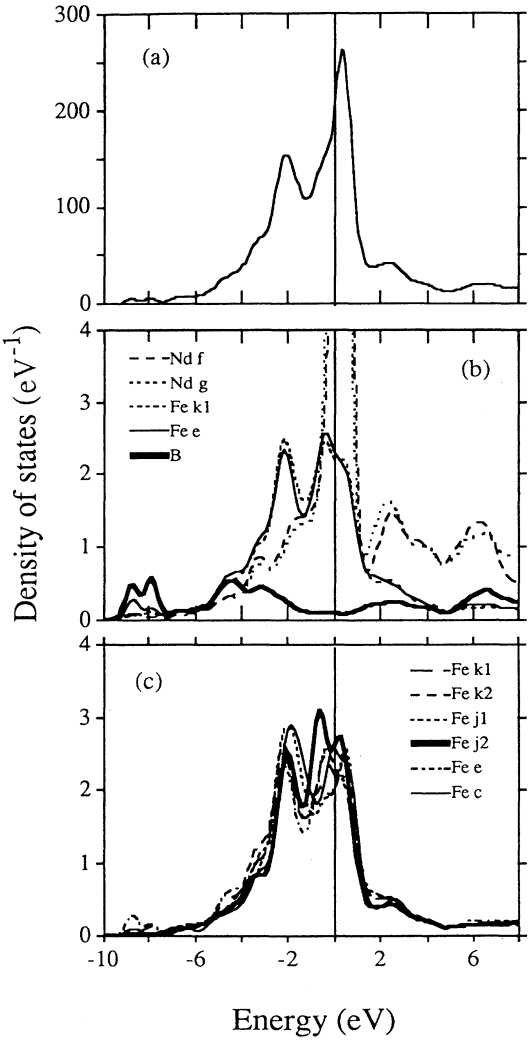

FIG. 2. (a) Total density of states (DOS) of paramagnetic $Nd_2Fe_{14}B$; (b) site-projected local density of states (LDOS) of each atom in the prism structure of paramagnetic $Nd_2Fe_{14}B$; (c) local density of states (LDOS) of six types of Fe atoms in paramagnetic $Nd_2Fe_{14}B$. Note that the LDOS peak of Fe(j_2) is the most prominent.

of $Nd_2Fe_{14}B$ in the paramagnetic phase. They are calculated at the experimental lattice constants of $a = 8.80$ Å and $c = 12.19$ Å. As mentioned above, the Nd f electrons in this case are considered as valence electrons, which yield the f-electron occupancies per Nd(f) and Nd(g) atoms of about 3.4 and 3.1, respectively. The Fe 3d-electron occupancy per Fe atom is 6.5–6.6, which is similar to that of the bcc bulk Fe ($\sim$ 6.6). It is found that there is slight charge depletion at the Fe(j_1) and Fe(c) atoms.

The total DOS of $Nd_2Fe_{14}B$ in Fig. 2(a) exhibits two pronounced peaks, one at $\sim$ 2 eV below the Fermi level (E_F) and the other near E_F. The peak at ~ -2 eV is mostly due to the Fe d bands, and the peak just above E_F is due to the Fe d and Nd f bands. In the paramagnetic phase, the DOS at E_F, $N(E_F)$, is very large [with $N(E_F)$=201.4/eV], to which the Nd 4f and Fe 3d bands mainly contribute. Such a large value of $N(E_F)$ suggests the possibility of a magnetic or structural phase transition. The magnetic phase transition can be qualitatively understood in terms of the exchange-correlation interactions in the Stoner theory of magnetism.[16] In $Nd_2Fe_{14}B$, the Stoner parameter S, defined as $N(E_F)I_{XC}$ with I_{XC} denoting the intra-atomic exchange-correlation integral, becomes larger than 1 ($S = 1.6$) due to the large value of $N(E_F)$, and thus ferromagnetic instability is expected to occur.

Figure 2(b) shows the projected local density of states (LDOS) at each atomic site of the trigonal prism structure (Fig. 1). A sharp and narrow band near E_F is due to mainly the 4f LDOS at Nd(f) and Nd(g) atoms, and other bands at higher binding energies are due to the Fe 3d LDOS at Fe(k_1) and Fe(e) atoms which overlap each other. The 5d LDOS of Nd atoms also exists in this energy range with a small weight near E_F. The weight distributions of the Fe(k_1) and Fe(e) 3d LDOS's look similar. The Fe(e) 3d LDOS shows a deeper valley at ~ -1.5 eV, which reflects that the hybridization of the Fe(e) band with other bands is larger than that of the Fe(k_1) band. The relatively low bands around -8 eV are mostly due to the B 2s bands with a mixture of Fe 4s bands. One can see that hybridization between B and Fe(e) atoms is rather large.

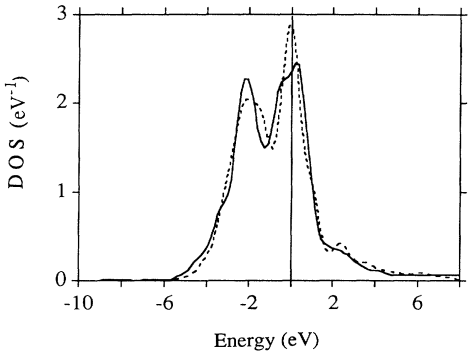

FIG. 3. Average Fe 3d DOS of $Nd_2Fe_{14}B$ (solid line) vs that of $NdFe_5$ (dashed line).

Figure 2(c) shows the LDOS at six types of Fe atoms. The overall shape of the LDOS is more or less the same for the six types of Fe atoms. A small structure around -8 eV is due to the hybridization interaction with B atoms. The LDOS at E_F is the largest for Fe(j_2), which is consistent with the fact that Fe(j_2) atoms are located far away from B atoms and that the distances to near neighbor Fe atoms are larger than those of other Fe atoms.[4] Such large LDOS's at E_F induce large Fe magnetic moments.

The B 2p bands spread widely between -6 and 8 eV, which are split into bonding and antibonding states below and above E_F, respectively, due to hybridization interactions with Fe 3d and Nd 5d bands. This result indicates that B atoms in this compound contribute to the stabilization of the structure through the hybridization bonding of B p with Fe d and Nd d bands. This feature is clearly seen in Fig. 3, which compares the average Fe 3d DOS of the $Nd_2Fe_{14}B$ with that of the unstable Nd-Fe intermetallic compound $NdFe_5$. Since the contribution of Nd f electrons to bonding is expected to be negligible, they are treated as core electrons in this calculation. Interestingly, in $NdFe_5$, the Fermi level is located right at the highest DOS peak position. Because of this very high DOS at E_F, $NdFe_5$ seems to be structurally unstable in nature. The B atoms in $Nd_2Fe_{14}B$ play a role to reduce $N(E_F)$ so as to stabilize the crystal structure, and such a role of B atoms in $Nd_2Fe_{14}B$ is similar to that observed in $NdFe_4B$.[17]

C. Spin-polarized calculation

Figure 4(a) shows the spin-polarized DOS of $Nd_2Fe_{14}B$ in the ferromagnetic phase. The DOS, which is large at E_F in the paramagnetic state, is now split into spin-up and spin-down DOS's due to an exchange-correlation interaction, resulting in the decrease in the DOS at E_F by about 27% [$N(E_F)$=147.7/eV]. In contrast to the paramagnetic state, the contribution of Fe 3d bands is very small in the spin-up DOS near E_F, but the contribution of Nd 4f bands is dominant. The spin-down bands near E_F are mostly due to Fe 3d bands. From this figure, the average exchange splitting for the Fe 3d bands is estimated to be 1.5–2 eV. Nd 4f spin-down bands are located at $\sim$ 2.3 eV above E_F due to band splitting. Figure 4(b) compares the LDOS's at Fe(j_2) and Fe(e) atoms in $Nd_2Fe_{14}B$ with the DOS of bcc bulk Fe. The bandwidth of the Fe(e) LDOS is larger and the exchange splitting of the Fe(j_2) LDOS is larger than that of bcc bulk Fe. Such differences are due to the hybridization with B atoms.

Table I summarizes the calculated magnetic moment of each atom in $Nd_2Fe_{14}B$. Nd 4f spin magnetic moments are $2.95\mu_B$ and $3.03\mu_B$ for Nd(f) and Nd(g) atoms, respectively. Spin magnetic moments due to s,p,d electrons polarize antiparallel to Nd 4f spin magnetic moments, resulting in $-0.32\mu_B$ for Nd(f) and $-0.31\mu_B$ for Nd(g). Thus the total spin magnetic moments become 2.63 for Nd(f) and $2.72\mu_B$ for Nd(g). As expected in the paramagnetic electronic structure, the spin magnetic moments of Fe(j_2) and Fe(c) atoms, $2.69\mu_B$ and $2.41\mu_B$, respectively, are much enhanced, compared to that of bcc bulk

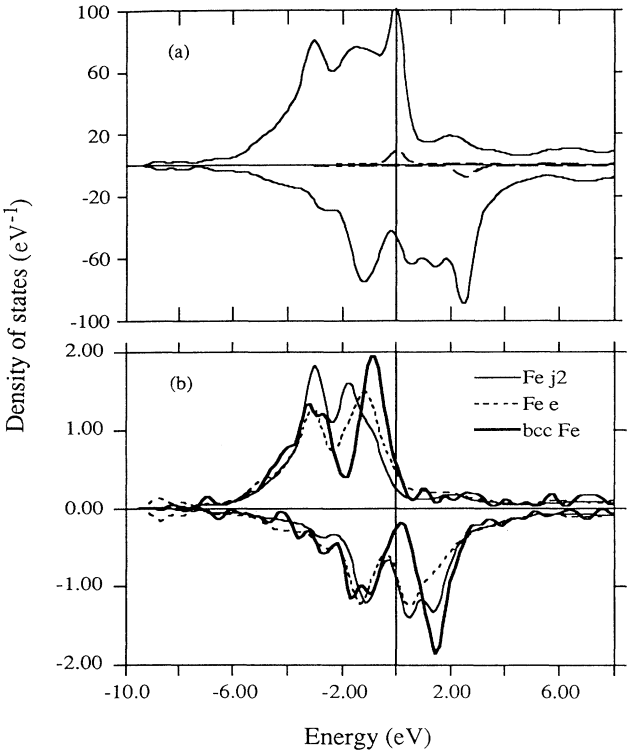

FIG. 4. (a) Total density of states of ferromagnetic $Nd_2Fe_{14}B$. Upper and lower curves correspond to spin-up and spin-down DOS's, respectively. Local density of states (LDOS) of Nd sites, which is exchange split, is also shown. (b) Local density of states (LDOS) of two types of Fe atoms, Fe(j_2) and Fe(e), in the ferromagnetic $Nd_2Fe_{14}B$, which are compared with the DOS of bcc bulk Fe.

Fe, 2.22μ_B, whereas Fe(e) atoms have the most reduced spin magnetic moment, 1.91μ_B. Such enhancement and reduction in magnetic moments are due to hybridization interactions between Fe and B atoms and local environment effects. Our calculated average spin magnetic moment per Fe atom, 2.15μ_B, is slightly smaller than the values of Gu and Ching,[8] 2.46μ_B, Jaswal,[11] 2.27μ_B, and Nordstroem, Johansson, and Brooks,[13] 2.35μ_B. Note that the result by Gu and Ching is a non-self-consistent one, and thus a direct comparison may be not appropriate. The deviation of our result from those of Jaswal and Nordstroem, Johansson, and Brooks seems to originate from the fact that interactions between Nd 4f and Fe 3d electrons are included in our calculations by treating Nd 4f electrons as valence electrons. In fact, our calculation with treating Nd 4f electrons as core electrons also yields larger magnetic moments for Fe atoms, as presented in Table I.

It is found that the trend of the calculated magnetic moments at different Fe sites agrees well with that of experimental data, as shown in Table I. Experimental magnetic moments, which are determined by neutron-diffraction[18] and Mössbauer effects,[19,20] are largest at the Fe(j_2) sites and smallest at the Fe(e) sites, respectively, in qualitative agreement with theoretical values. There are some quantitative differences between theoretical and experimental magnetic moments, and even two experiments yield different magnetic moments: The reported value for the average magnetic moment per Fe atom is $\sim 2.56\mu_B$ by neutron scattering, whereas it is in the range of (2.16–2.28)μ_B by Mössbauer experiments. Thus more experimental studies are a prerequisite for a better understanding of such discrepancies.

III. *Nd 4f* PES SPECTRA

Figure 5(a) shows the PES spectra for a polycrystalline compound of $Nd_2Fe_{14}B$, obtained using synchrotron radiation. The methods for sample preparation and PES measurements are same as those described in Ref. 21. Our PES data obtained with photon energies of around 40 eV do not show any O and/or C contamination. The PES data are taken at $\sim$ 60 K, far below the Curie temperature, 585 K. The total instrumental resolution [full width at half maximum (FWHM)] is about 0.3 eV for the PES spectra reported in this paper. All the PES spectra were normalized to the incident photon flux.

TABLE I. Magnetic moment (in μ_B) of each atom in $Nd_2Fe_{14}B$. Calculated results by Gu and Ching (Ref. 8), Jaswal (Ref. 11), and Nordstroem, Johansson, and Brooks (Ref. 13), as well as minimum and maximum experimental values from Refs. 18–20 are presented for comparison.

	Nd(f)	Nd(g)	Fe(k_1)	Fe(k_2)	Fe(j_1)	Fe(j_2)	Fe(e)	Fe(c)	B
Theory[a]	2.63	2.72	2.00	2.08	2.04	2.69	1.91	2.41	-0.17
Theory[b]	-0.38	-0.37	2.09	2.17	2.17	2.72	1.97	2.47	-0.18
Theory[c]	3.01	3.04	2.15	2.28	2.48	3.40	1.99	2.97	0.36
Theory[d]	-0.55	-0.52	2.15	2.18	2.12	2.74	2.13	2.59	-0.20
Theory[e]	-0.57	-0.53	2.35	2.23	2.10	2.86	2.15	2.45	-0.18
Expt.(min)[f]			2.08	2.16	2.06	2.43	2.00	1.97	
Expt.(max)[f]			2.60	2.60	2.30	2.85	2.28	2.75	

[a] This work with treating Nd f electrons as valence electrons.
[b] This work with treating Nd f electrons as core electrons.
[c] Ref. 8.
[d] Ref. 11.
[e] Ref. 13.
[f] Taken from Refs. 18–20.

TABLE II. Fitting parameters for the extracted Nd $4f$ PES spectrum shown in Fig. 5(b). Those values for the pure Nd metal are taken from Ref. 23. 2γ corresponds to the FWHM (full width at half maximum) of the Lorentzian broadening, and α denotes the asymmetry factor. Also given are the surface core-level shift (Δ_{SCS}) of the Nd $4f^2$ final-state peaks and the bulk-to-surface intensity ratio (I_B/I_S).

	Bulk		Surface			
	2γ (eV)	α	2γ (eV)	α	Δ_{SCS} (eV)	I_B/I_S
$Nd_2Fe_{14}B$	0.70	0.12	0.86	0.10	0.45	1.20 ($h\nu = 128$ eV)
Nd metal	0.76	0.12	1.0	0.10	0.5	1.5 ($h\nu = 100$ eV)

Photon energies of $h\nu = 128$ eV and $h\nu = 121$ eV correspond to a maximum and minimum of the Fano resonance[22] in the cross section for Nd $4f$ emission, respectively. [The spectrum for $h\nu = 121$ eV (solid lines) will be discussed in detail in Fig. 7.] It is possible to extract the Nd $4f$ emission by subtracting the spectrum at the Fano minimum from that at the Fano maximum. The difference curve, shown as the dashed lines, corresponds to the extracted Nd $4f$ spectrum. The main peak at ~ -5.5 eV can be identified as the trivalent (Nd^{3+}) emission, corresponding to the $4f^3 \rightarrow 4f^2$ transition. The FWHM of the trivalent $4f$ PES peaks for $Nd_2Fe_{14}B$, which is ~ 2.4 eV, appears to be larger than that for pure Nd metal (~ 1.8 eV).[23] This is because there are more components underneath the trivalent $4f$ peaks for $Nd_2Fe_{14}B$ than for Nd metal, as will be shown below by deconvolution of the Nd $4f$ PES spectrum.

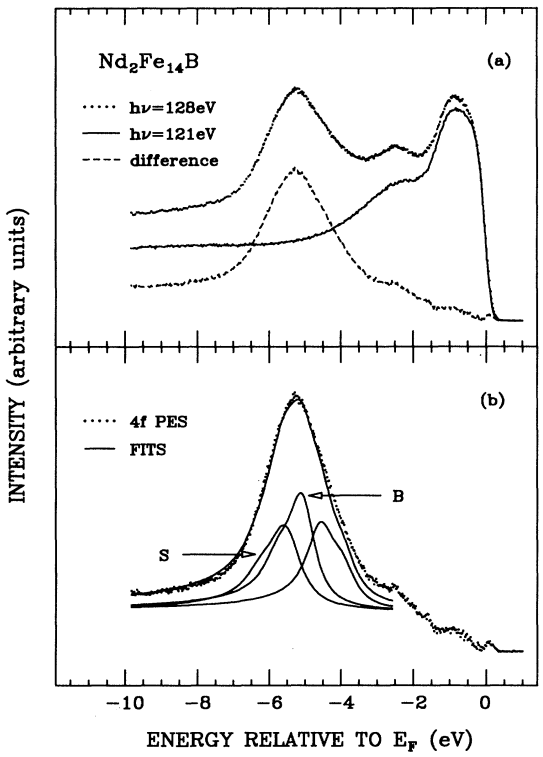

FIG. 5. (a) Valence-band photoemission (PES) spectra of $Nd_2Fe_{14}B$. Dots and solid lines represent the PES spectrum taken at $h\nu = 128$ eV and 121 eV, respectively, from which the inelastic backgrounds are subtracted. The dashed line denotes the difference between these two spectra. The feature at ~ -5 eV can be identified as the $4f^3 \rightarrow 4f^2$ transition. (b) Dots denote the difference spectrum, which is same as that in (a) denoted with dashed lines. The solid lines are the theoretical fits. The fits are obtained with $4f^3 \rightarrow 4f^2$ multiplet structures calculated as in Ref. 29, in which the energy scale is expanded by a factor of 1.1 to obtain the best fits. B and S represent the bulk and surface peaks, respectively.

The main peak of the extracted Nd $4f$ PES spectrum is fitted using the $4f^2$ final-state multiplet structures calculated from the coefficients of fractional parentage,[24] and the results are shown as solid lines in Fig. 5(b). We have multiplied the energy scaling factor of 1.1 to the atomic theoretical multiplet splittings to account for solid-state effects. In the curve fittings, the final-state multiplets are assumed to have Doniach-Sunjic line shapes and they are convolved with a Lorentzian to simulate broadening due to the finite lifetime of the $4f$ hole.[25] The peaks are further convolved with a Gaussian to simulate experimental resolution. The labels of B and S in Fig. 5(b) correspond to the bulk and surface peaks, respectively, of the $4f^2$ final-state ("trivalent") multiplet structures in Nd metal.

The fitting parameters are summarized in Table II. 2γ corresponds to the FWHM of the Lorentzian broadening, α denotes the asymmetry factor, Δ_{SCS} denotes the surface $4f$ level shift, and I_B/I_S denotes the intensity ratio of the bulk to the surface $4f^2$ final-state multiplets. The parameter values for Nd metal, taken from Ref. 23, are also presented for comparison. One can see that the parameter values for $Nd_2Fe_{14}B$ are similar to those for Nd metal. The separation of bulk and surface $4f^2$ final-state multiplet structures (Δ_{SCS}) is ~ 0.45 eV, which is comparable to, but slightly smaller than that for Nd metal (~ 0.5 eV). This phenomenon may be understood in terms of the thermochemical model by Johansson and Martensson,[26] considering that the measured location of the Nd $4f$ PES peak maximum (~ -5.2 eV) in $Nd_2Fe_{14}B$ is shifted to higher binding energy from that in Nd metal (~ -5.0 eV).

It is important that an extra set of components, with binding energies of -3.9 eV and -4.5 eV, is required to fit the Nd $4f$ PES spectrum for $Nd_2Fe_{14}B$, in addition to the two sets of bulk and surface $4f^2$ peaks. As mentioned above, these extra components cause the FWHM of the trivalent peaks for $Nd_2Fe_{14}B$ to be larger than that for

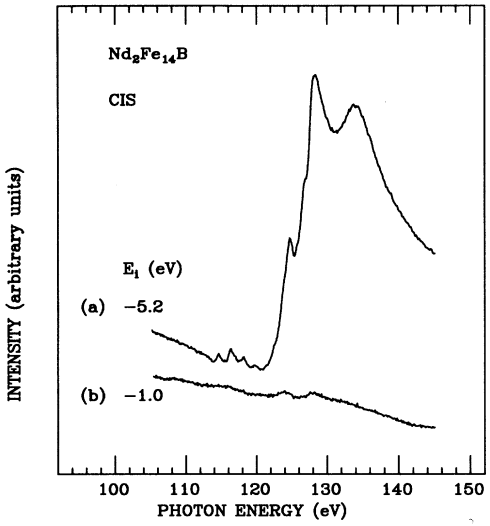

FIG. 6. CIS spectra of $Nd_2Fe_{14}B$ for states with initial-state energies (E_i) at −5.2 eV and −1.0 eV, respectively.

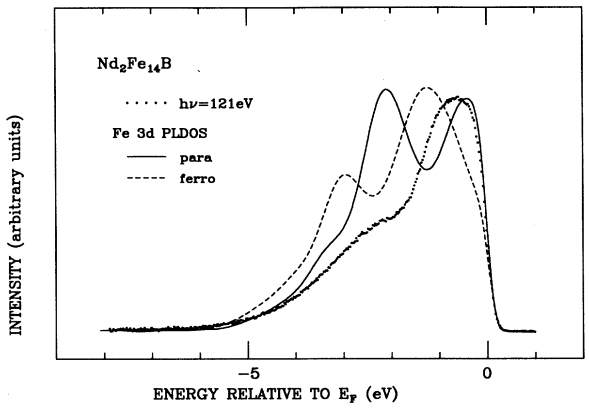

FIG. 7. Comparison of the experimental valence-band PES spectrum with the theoretical PLDOS. Dots can be regarded to represent experimental Fe 3*d* PES spectrum of $Nd_2Fe_{14}B$, which is taken with $h\nu = 121$ eV. Inelastic backgrounds have been subtracted from the $h\nu = 121$ eV spectrum. The solid and dashed lines represent the calculated Fe 3*d* PLDOS for paramagnetic and ferromagnetic phases, respectively. A Gaussian broadening of 0.3 eV (FWHM) was used to simulate the experimental resolution.

Nd metal. Although the origin for such extra components around −4 eV is not clear at the moment, it is plausible that some of the Nd 4*f* spectral weight is transferred toward E_F due to the hybridization between Nd 4*f* and Fe 3*d* states.[27]

Figure 6 shows the constant initial-state (CIS) spectra for initial-state energies E_i at −5.2 eV and −1.0 eV, respectively, which represent the photon energy dependence of the Nd 4*f* states and the state near E_F. The Nd 4*f* CIS spectrum with $E_i = -5.2$ eV shows structures which are due to the $4d^9 4f^4$ intermediate-state multiplet structures.[24,28] The CIS line shape with $E_i = -5.2$ eV is nearly identical to that for Nd metal,[29] for which the Nd valence is close to 3+. This finding implies that the Nd valence for the state near $E_i = -5.2$ eV is near trivalent in $Nd_2Fe_{14}B$. We have found that the CIS spectra, which are obtained with different values of E_i between −4 and −10 eV, exhibit similar line shapes (not shown here). From this it is expected that the Nd valence does not change for E_i over −4 to −10 eV. In contrast, the CIS spectrum with $E_i = -1.0$ eV shows negligible resonance, which indicates a lack of Nd 4*f* components near E_F. This is consistent with Fig. 5, in which negligible Nd 4*f* spectral intensity is observed near E_F. To summarize, Fig. 6 provides two pieces of evidence: (i) The contribution of Nd 4*f* states to the DOS near E_F is negligible, and (ii) the Nd valence in $Nd_2Fe_{14}B$ is close to trivalent. These findings are consistent with the magnetic properties which exhibit the localized 4*f* moment of trivalent Nd ions.[4]

IV. COMPARISON OF THE Fe 3*d* PES SPECTRA WITH THE CALCULATED PLDOS

Figure 7 shows the valence-band PES spectrum, taken at $h\nu = 121$ eV, corresponding to the Fano minimum of the Nd 4*f* photoionization cross section. The spectrum at this photon energy can be considered to represent the Fe 3*d* emission because (i) the Nd 4*f* emission is suppressed due to the Fano minimum, (ii) the Fe 3*d* photoionization cross section is relatively larger than those of Nd 5*d* and B *s*, *p* electrons at this photon energy,[30] (iii) the number of Fe 3*d* electrons is dominant compared to other electrons in $Nd_2Fe_{14}B$.

Note several interesting features in the Fe 3*d* PES spectrum. First, the spectrum is rather broad, as compared to the Nd 4*f* PES spectrum, and no pronounced satellite structures are observed, suggesting that the Fe 3*d* Coulomb correlation energies are smaller than the Fe 3*d* bandwidths in $Nd_2Fe_{14}B$. Second, the peak in the Fe 3*d* PES spectrum is close to E_F, resulting in a large spectral weight near E_F. This feature is in sharp contrast with that of the Nd 4*f* PES spectra of Figs. 5 and 6. Therefore it is concluded that the DOS near E_F in $Nd_2Fe_{14}B$ is determined mainly by Fe 3*d* electrons. Third, the separation between the peak maximum (at ∼ −0.5 eV) and the broad bump at higher binding energy (at ∼ −2.5 eV) is about 2 eV.

Figure 7 also provides a comparison between the Fe 3*d* valence-band PES spectrum and the calculated angular-momentum-projected local density of states (PLDOS). Solid and dashed lines represent the calculated Fe 3*d* PLDOS for the paramagnetic and ferromagnetic phases, respectively, which are convolved with a Gaussian of 0.3 eV FWHM to simulate the experimental resolution. For the ferromagnetic 3*d* PLDOS, occupied parts of the calculated Fe 3*d* majority- and minority-spin PLDOS's are summed and averaged over sites, because our PES spectrum is not spin resolved nor site resolved.

The comparison of Fig. 7 shows that the widths of the occupied part of the calculated Fe 3*d* PLDOS are in rather good agreement with the experimental Fe 3*d* PES spectrum. This agreement supports the fact that the Fe 3*d* Coulomb correlation energies are smaller than the Fe

$3d$ bandwidths in $Nd_2Fe_{14}B$. Note that the separation between the peak maximum and the bump at higher binding energy in the PES spectrum, which can be a measure of the exchange splitting for the Fe $3d$ bands, is comparable to that in the theoretical Fe $3d$ PLDOS. However, the peak positions of the theoretical $3d$ PLDOS are somewhat different from those of the $3d$ PES spectrum. One possible explanation for this small deviation in the peak position can be due to the finite temperature at which experimental data are taken. The magnitude of the exchange splitting is dependent on the temperature,[31] and so the peak of the experimental data at finite temperature is expected to be located between the calculated peak positions of paramagnetic and ferromagnetic results. In fact, the experimental peak position is located between the two peaks of the paramagnetic and ferromagnetic Fe $3d$ PLDOS's. Noticeable discrepancies are also observed in the weight distribution. Such discrepancies could be partially due to matrix element effects, which are not included in the theory. Thus the local-density-approximation (LDA) band-structure calculations can be regarded to provide a reasonable agreements between the Fe $3d$ PLDOS and the measured Fe $3d$ PES spectrum for $Nd_2Fe_{14}B$. These agreements also suggests that the Fe $3d$ magnetism in $Nd_2Fe_{14}B$ may well be described by the itinerant magnetism of Fe $3d$ electrons.

It will be interesting to observe the experimental evidence for the hybridization between B s,p and Fe $3d$ electrons, as has been predicated by band-structure calculations. B s,p states are predicted to be in the energy range from -10 to over 8 eV by band-structure calculations. Unfortunately, the photoionization cross sections for B s,p electrons are very small relative to those of other states for the photon energies used in this study.[30] Thus it is not possible to compare the theoretical B s,p PLDOS with the B s,p PES spectrum in this work.[32]

V. CONCLUSIONS

The electronic and magnetic structures of $Nd_2Fe_{14}B$ have been investigated by performing self-consistent LDA band-structure calculations and photoemission spectroscopy measurements. Employing the LMTO band method, we have obtained electronic band structures for both paramagnetic and ferromagnetic phases of $Nd_2Fe_{14}B$. It is found that B atoms play an important role in stablizing the structure through hybridization bonding with the near-neighbor Fe and Nd atoms and that B atoms substantially reduce the magnetic moments of neighbor Fe atoms. The average magnetic moment of Fe atoms in the ferromagnetic phase is estimated to be $2.15\mu_B$. Fe atoms at the j_2 site, which are located farthest from the B atom and surrounded by 12 nearest-neighbor Fe atoms, have the largest magnetic moment, $2.7\mu_B$, while Fe atoms at the e site, which interact most strongly with B atoms, have the smallest magnetic moment, $1.9\mu_B$.

Both the Nd $4f$ PES and CIS spectra show that there is negligible contribution of Nd $4f$ states to the DOS near E_F and that the Nd valence is near trivalent in $Nd_2Fe_{14}B$. This finding confirms the observation that Nd $4f$ electrons exhibit localized $4f$ magnetic moments of trivalent rare-earth ions. The FWHM of the $4f$ PES peak in $Nd_2Fe_{14}B$ is larger than that in pure Nd metal, which is considered to reflect the hybridization interaction between Nd $4f$ and Fe $3d$ states. The measured Fe $3d$ PES spectrum shows a large spectral intensity near E_F with its main peak at about 0.5 eV below E_F. The Fe $3d$ PES line shape is the rather broad with no pronounced satellite structures, indicating the rather delocalized nature of Fe $3d$ states. Such features are consistent with the finding that the bandwidth of the measured Fe $3d$ PES spectrum is in reasonably good agreement with that of the calculated Fe $3d$ PLDOS.

ACKNOWLEDGMENTS

We thank S.-J. Oh for providing us with the fitting program. This work has been supported by the Korean Science and Engineering Foundation (KOSEF) under Contract No. 921-0200-005-2, by the Center for the Advanced Materials Physics at POSTECH, and by the Pohang Light Source (PLS). The experiment was performed at the U.S. Synchrotron Radiation Center, which is supported by the U.S. National Science Foundation.

[1] *Ferromagnetic Materials, A Handbook on the Properties of Magnetically Ordered Substances*, edited by E.P.Wohlfarth and K.H.J. Buschow (North-Holland, Amsterdam, 1988).
[2] R.J. Parker, *Advances in Permanent Magnetism* (Wiley, New York, 1990).
[3] *Physical Properties on $R_2Fe_{14}B$-based Alloys in Handbook on the Physics and Chemistry of Rare-Earths*, edited by K.A. Gschneidner and L. Eyring (North-Holland, Amsterdam, 1989), Vol. 12, Chap. 82.
[4] J.F. Herbst, Rev. Mod. Phys. **63**, 819 (1991), and references therein.
[5] J. Inoue and M. Shimizu, J. Phys. F **16**, 1051 (1986).
[6] T. Itoh, K. Hikosaka, H. Takahashi, T. Ukai, and N. Mori, J. Appl. Phys. **61**, 3430 (1987).
[7] B. Szpunar, W.E. Wallace, and J. Szpunar, Phys. Rev. B **36**, 3782 (1987).
[8] Z.Q. Gu and W.Y. Ching, Phys. Rev. B **36**, 8530 (1987).
[9] X.-F. Zhong and W.Y. Ching, J. Appl. Phys. **67**, 4768 (1990), and references therein.
[10] D.J. Sellmyer, M.A. Engelhardt, S.S. Jaswal, and A.J. Arko, Phys. Rev. Lett. **60**, 2077 (1988).
[11] S.S. Jaswal, Phys. Rev. B **41**, 9697 (1990).
[12] O.K. Andersen, Phys. Rev. B **12**, 3060 (1975); H.L. Skriver, *The LMTO Method*, Springer Series in Solid State Sciences Vol. 41 (Springer-Verlag, Berlin, 1984).
[13] L. Nordstroem, B. Johansson, and M.S.S. Brooks, J. Appl. Phys. **69**, 5708 (1991).
[14] C. Woodward, B.I. Min, R. Benedek, and J. Garner, Phys. Rev. B **39**, 4853 (1989).
[15] P. Hohenberg and W. Kohn, Phys. Rev. **136**, B864 (1964); W. Kohn and L.J. Sham, *ibid.* **140**, A1133 (1965).
[16] J.F. Janak, Phys. Rev. B **16**, 255 (1977).

[17]B.I. Min and Y.R. Jang, J. Korean Magn. Soc. **1**, 6 (1991).
[18]D. Givord, H.S. Li, and F. Tasset, J. Appl. Phys. **57**, 4100 (1985).
[19]R. Fruchart, P. L'Heritier, P. Dalmas de Reotier, D. Fruchart, P. Wolfers, J.M.D. Coey, L.P. Ferreira, R. Guillen, P. Vulliet, and A. Youamce, J. Phys. F **17**, 483 (1987).
[20]H. Onodera, H. Yamauchi, M. Yamada, H. Yamamoto, M. Sagawa, and S. Hirosawa, J. Magn. Magn. Mater. **68**, 15 (1987).
[21]J.-S. Kang, J.H. Hong, J.I. Jeong, S.D. Choi, C.J. Yang, Y.P. Lee, C.G. Olson, B.I. Min, and J.W. Allen, Phys. Rev. B **46**, 15689 (1992).
[22]U. Fano, Phys. Rev. **124**, 1866 (1961).
[23]F. Gerken, A.S. Flodstrom, J. Barth, L.I. Johansson, and C. Kunz, Phys. Scr. **32**, 43 (1985).
[24]F. Gerken, J. Phys. F **13**, 703 (1983).
[25]G.D. Mahan, *Many-Particle Physics* (Plenum, New York, 1981), p. 746.
[26]B. Johansson and N. Martensson, in *Handbook on the Physics and Chemistry of Rare-Earths*, edited by K.A. Gschneidner, L.R. Eyring, and S. Hufner (North-Holland, Amsterdam, 1987), Vol. 10, p. 361.
[27]J.W. Allen, S.-J. Oh, O. Gunnarsson, K. Schoenhammer, M.B. Maple, M.S. Torikachvili, and I. Lindau, Adv. Phys. **35**, 275 (1986).
[28]J.K. Lang, Y. Baer, and P.A. Cox, J. Phys. F **11**, 121 (1981).
[29]F. Gerken, Ph.D. thesis, University of Hamburg, 1982.
[30]J.J. Yeh and I. Lindau, At. Data Nucl. Data Tables **32**, 1 (1985).
[31]B. Kim, A.B. Andrew, J.L. Erskine, K. Kim, and B.N. Harmon, Phys. Rev. Lett. **50**, 1931 (1992).
[32]This is not due to the depletion of B at the surface of our $Nd_2Fe_{14}B$ sample. In fact, it is likely that B might have diffused to the surface. We have found that the boron to iron concentration of our $Nd_2Fe_{14}B$ sample is about 1/10 from the core-level PES measurements, which is comparable to the bulk concentration considering uncertainties in estimating the atomic concentration.